INTERNATIONAL JOURNAL FOR NUMERICAL METHODS IN FLUIDS, VOL. 26, 125–143 (1998)

COMPUTING THE FLOW AROUND A MOVING PROFILE BY NUMERICALLY INTEGRATING THE NAVIER–STOKES EQUATIONS

LAURENTIU PASCU

STRAERO S.A., Bd Pacu 220, Bucharest 77358, Romania and Université Pierre et Marie Curie, Paris, France

SUMMARY

A vorticity velocity formulation is proposed for the solution of the equations for viscous flow around a moving profile. A non-inertial reference frame is used and the velocities are computed from a Poincaré integral formula. The studies are directed towards the need to understand helicopter blade aerodynamics. Worked examples are given which validate the method and programme for laminar flows, at least for low Reynolds numbers. © 1998 John Wiley & Sons, Ltd.

Int. J. Numer. Meth. Fluids, **26**: 125–143 (1998)

KEY WORDS: Navier–Stokes; unsteady separated flow; laminar flow; vorticity; non-inertial frame

INTRODUCTION

The area of unsteady separated flow management has been receiving considerable attention in recent years.[1–4] In our case such studies are motivated by the need to understand helicopter blade aerodynamics. The present paper proposes an approach somewhat different from those in the present literature. We use a non-inertial reference frame having the advantage of a time-independent computational domain and mesh. Moreover, following Reference 5, we employ a vorticity velocity formulation in which velocities are computed from a Poincaré integral formula. In the theoretical part of the paper we show that the new non-inertial frame formulation is very much like the existing one, allowing the use of the same numerical procedures. As suggested in Reference 6, the computational domain is conformally represented on the exterior of a circle, allowing an explicit formula for boundary vorticity computation and also providing a good mesh for the finite difference method employed for the transport and diffusion equation. The domain and boundary integrals involved in velocity computation are evaluated in the transformed plane by Fourier series expansions in the polar angle direction and by the trapezoidal rule in the radial direction. Some test flows are analysed and a comparison with experimental and numerical data is made.

INTEGRODIFFERENTIAL FORMULATION

Let us consider the general problem of an aerodynamic profile translating and rotating in an incompressible viscous fluid at rest at infinity. Let $x'O'y'$ be a reference frame related to the fluid and xOy another one related to the moving profile. We shall denote all quantities measured in the first reference frame with a prime. For simplicity we shall also denote, when possible, the vectors orthogonal to the flow plane (free or bounded vorticity, rotation angle, angular velocity, etc.) only by their significant scalar component.

CCC 0271–2091/98/020125–19 $17.50

Received May 1995
Revised November 1995

The movement of the profile is given by specifying $\vec{r}'_0$ and θ as functions of time over the considered interval $[0, T]$, with $T > 0$ (see Figure 1). The relationship between the velocities in the reference frames thus defined is then:

$$\vec{v}(\vec{r}', t) = \vec{v}(\vec{r}, t)\frac{\mathrm{d}\vec{r}'_0}{\mathrm{d}t}(t) + \vec{\Omega}(t) \times \vec{r}, \tag{1}$$

with $\vec{r}$ and $\vec{r}'$ the corresponding position vectors and $\Omega(t)$ given by

$$\Omega(t) = \frac{\mathrm{d}\theta}{\mathrm{d}t}(t). \tag{2}$$

Let D be the domain exterior to the profile (which is assumed of class $\mathscr{C}^{1,1}$, eventually excepting the trailing edge) considered in its reference frame, so D is independent of time. The continuity and Navier-Stokes equations for uniform density ρ and kinematic viscosity ν can be written in terms of velocity and pressure as

$$\operatorname{div} \vec{v} = 0, \tag{3a}$$

$$\operatorname{rot} \vec{v} = \vec{\omega}, \tag{3b}$$

$$\frac{\partial \vec{v}}{\partial t} + \operatorname{grad}\left(\frac{v^2}{2} + \frac{p}{\rho}\right) + \vec{\omega} \times \vec{v} = \vec{f}_{\mathrm{i}} + \nu\Delta\vec{v}, \tag{3c}$$

with $\vec{v} \in \mathscr{C}^1(D \times [0, T])$ having continuous second-order spatial derivatives on D, $p \in \mathscr{C}^0(D \times [0, T])$ having continuous first-order spatial derivatives on D, and $\vec{f}_i$, the inertial mass forces, given by

$$\vec{f}_{\mathrm{i}} = -\frac{\mathrm{d}^2\vec{r}'_0}{\mathrm{d}t^2} - \frac{\mathrm{d}\vec{\Omega}}{\mathrm{d}t} \times \vec{r} - 2(\Omega \times \vec{v}) - \vec{\Omega} \times (\vec{\Omega} \times \vec{r}). \tag{4}$$

The PDE (3) is subject to the following boundary and initial conditions:

$$\vec{v}(\vec{r}, t) = 0 \tag{5}$$

on the profile surface;

$$\vec{v}(\vec{r}', t) = O(1/r), \tag{6}$$

$$p(\vec{r}, t) = p_\infty + O(1/r) \tag{7}$$

for $\vec{r} \to \infty$ and $t \in [0, T]$; and

$$\vec{v}(r, 0) = \vec{v}_0(\vec{r}) \tag{8}$$

for $t = 0$ and $\vec{r} \in D$.

Further, (6) is equivalent (by (1)) to

$$\vec{v}(\vec{r}, t) = -\frac{\mathrm{d}\vec{r}'_0}{\mathrm{d}t}(t) - \vec{\Omega}(t) \times \vec{r} + O(1/r) \quad \text{for} \quad \vec{r} \to \infty \tag{9}$$

in terms of relative velocity $\vec{v}$.

In order to derive an analogue for the vorticity transport and diffusion equation in the non-inertial reference frame, we shall take the curl of equation (3b). We obtain

$$\frac{\partial \vec{\omega}}{\partial t} + (\vec{v} \operatorname{grad})\vec{\omega} = -2\frac{\mathrm{d}\vec{\Omega}}{\mathrm{d}t} + \nu\Delta\vec{\omega}. \tag{10}$$

By considering the fact that the velocity correspondence (1) implies

$$\vec{\omega}' = \vec{\omega} + 2\vec{\Omega}, \tag{11}$$

we have

$$\frac{\partial \vec{\omega}}{\partial t} + (\vec{v} \operatorname{grad})\vec{\omega}' = \nu\Delta\vec{\omega}', \tag{12}$$

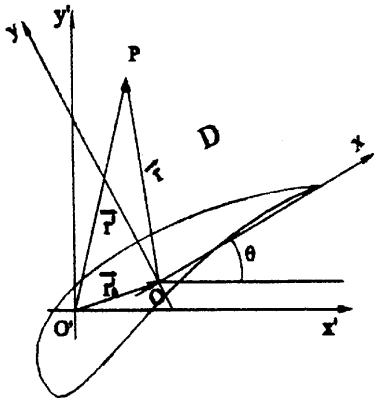

Figure 1

which is identical with the transport and diffusion equation for inertial reference frames, with the exception that now the advected and diffused quantity is the vorticity in the fixed frame while the advection velocity is related to the moving one.

Following the idea presented in Reference 5, we shall use an integral formula derived from the Poincaré identity to compute velocities in the region of interest. For this we need a supplementary assumption on $\vec{\omega}'$, namely

$$\vec{\omega}' = O(1/r^2) \quad \text{for} \quad r \to \infty \quad \text{and} \quad t \in [0, T]. \tag{13}$$

By considering the ball centred on the origin O and with radius R sufficiently large to include the profile, writing the Poincaré identity for the outside of the profile and the inside of the ball yields, after taking the limit for $R \to \infty$ and making use of (13),

$$\begin{aligned} \vec{v}(\vec{}, t) = &- \frac{\mathrm{d}\vec{r}_0'}{\mathrm{d}t}(t) - \vec{\Omega}(t) \times \vec{r} + \frac{1}{2\pi} \int\int_{R^2} \frac{\vec{\omega}(\vec{r}_1, t) \times (\vec{r} - \vec{r}_1)}{|\vec{r} - \vec{r}_1|^2} \mathrm{d}x_1 \mathrm{d}y_1 \\ &+ \frac{1}{2\pi} \int_{\partial D} \frac{[\vec{n}_1 \times (\vec{v}(\vec{r}_1, t)] \times (\vec{r} - \vec{r}_1)}{|\vec{r} - \vec{r}_1|^2} \mathrm{d}s_1 + \frac{1}{2\pi} \int_{\partial D} \frac{[\vec{n}_1 \cdot \vec{v}(\vec{r}_1, t)](\vec{r} - \vec{r}_1)}{|\vec{r} - \vec{r}_1|^2} \mathrm{d}s_1, \end{aligned} \tag{14}$$

where $\vec{n}_1$ points outside the profile, $\vec{\omega}'$ has been extended to the interior of the profile (CD) according to

$$\vec{\omega}'(\vec{r}, t) = \begin{cases} \vec{\omega}(\vec{r}, t) & \text{in } D, \\ 2\vec{\Omega}(t) & \text{in } CD \end{cases} \tag{15}$$

and (3a) was taken into account.

We cannot impose both $\vec{v} \cdot \vec{n} = 0$ and $\vec{v} \times \vec{n} = 0$ on ∂D in (14) according to (5), because this will not render zero velocity on the left-hand side for points on ∂D, except for particular values of $\vec{\omega}'$. As in Reference 5, only $\vec{v} \cdot z\vec{n} = 0$ is retained and a bounded vorticity layer of intensity

$$\vec{\gamma}(\vec{r}, t) = \vec{n} \times \vec{v}(\vec{r}, t) \tag{16}$$

is placed on ∂D, which is equivalent to considering a discontinuity of the tangential velocity of the same magnitude. This discontinuity will be removed later when the boundary condition for vorticity is imposed.

By taking the limit of (14) for $\vec{r} \to \vec{r}_{\mathrm{p}} \in \partial D$, one obtains a Fredholm integral equation of the second kind for $\vec{\gamma}$:

$$\tfrac{1}{2}\vec{\gamma}(\vec{r}_{\mathrm{p}}, t) - \frac{1}{2\pi}\vec{n}_{\mathrm{p}} \times \int_{\partial D} \frac{\vec{\gamma}(\vec{r}_1, t) \times (\vec{r}_{\mathrm{p}} - \vec{r}_1)}{|\vec{r}_{\mathrm{p}} - \vec{r}_1|^2}\,\mathrm{d}s_1$$

$$= \vec{n}_{\mathrm{p}} \times \left(-\frac{\mathrm{d}\vec{r}_0'}{\mathrm{d}t}(t) - \vec{\Omega}(t) \times \vec{r}_{\mathrm{p}} + \frac{1}{2\pi}\int\int_{R^2} \frac{\vec{\omega}(\vec{r}_1, t) \times (\vec{r}_p - \vec{r}_1)}{|\vec{r}_{\mathrm{p}} - \vec{r}_1|^2}\,\mathrm{d}x_1\mathrm{d}y_1 \right), \tag{17}$$

where $\vec{n}_{\mathrm{p}}$ is the outward normal vector to the profile surface at point $\vec{r}_{\mathrm{p}}$. As is well known, (17) admits an infinity of solutions of the form

$$\gamma = \gamma_0 + C\gamma_R \tag{18}$$

where $C \in \mathbb{R}$ and $\vec{\gamma}_R$ is numerically equal to the source distribution giving the Robin potential for the profile. We shall see later, in the section on the pressure computation procedure, how it is possible to select the proper solution, i.e. to determine the value of C.

With $\vec{\gamma}$ known, (14) becomes

$$\vec{v}(\vec{r}, t) = -\frac{\mathrm{d}\vec{r}_0'}{\mathrm{d}t}(t) - \vec{\Omega}(t) \times \vec{r} + \frac{1}{2\pi}\int\int_{R^2} \frac{\vec{\omega}(\vec{r}_1, t) \times (\vec{r} - \vec{r}_1)}{|\vec{r} - \vec{r}_1|^2}\,\mathrm{d}x_1\mathrm{d}y_1 + \frac{1}{2\pi}\int_{\partial D} \frac{\vec{\gamma}(\vec{r}_1, t) \times (\vec{r} - \vec{r}_1)}{|\vec{r} - \vec{r}_1|^2}\,\mathrm{d}s_1. \tag{19}$$

PRESSURE COMPUTATION

Once the solution of our problem in the vorticity–velocity formulation has been found, we must revert to equation (3) to compute pressure values, which is important for almost all applications. Although it seems possible by use of the known pressure gradient over all the computational domain, this is not the best way, because the accumulation of numerical errors may lead to different values for the same point, depending on the integration path (see e.g. Reference 7, p. 180). A better method consists of considering a Neumann problem for the Poisson equation that can be derived by applying the divergence operator to equation (3c).

For our case, since we are interested in a problem that can be confined to the viscous region of the flow (i.e. which has solutions that can be written in terms of surface and single-layer potentials), we put (3c) in the form

$$\frac{\partial \vec{v}}{\partial t} + \operatorname{grad} H = -\vec{\omega}' \times \vec{v} - \frac{\mathrm{d}^2\vec{r}_0'}{\mathrm{d}t^2} - \frac{\mathrm{d}\vec{\Omega}}{\mathrm{d}t} \times \vec{r} + \vec{\Omega} \times \frac{\mathrm{d}\vec{r}_0'}{\mathrm{d}t} + \nu\Delta\vec{v}, \tag{20}$$

with H, a Bernoulli-type variable, given by

$$H = \frac{p}{\rho} + \frac{v^2}{2} - \frac{p_\infty}{\rho} - \frac{1}{2}\left(\frac{\mathrm{d}\vec{r}_0'}{\mathrm{d}t} + (\vec{\Omega} \times \vec{r})\right)^2. \tag{21}$$

From (20) we derive

$$-\Delta H = \operatorname{div}(\vec{\omega}' \times \vec{v}) \tag{22}$$

and from (7) and (8) it is easy to see that

$$H = O(1) \quad \text{as} \quad r \to \infty \tag{23}$$

As far as the Neumann boundary condition is concerned, we shall take the scalar product of (20) by $\vec{n}_1$, the normal vector corresponding to point $\vec{r}_1 \in \partial D$, and pass to the limit for $\vec{r} \to \vec{r}_1$. We obtain

$$\frac{\partial H}{\partial n} = \omega' \gamma - \vec{n} \cdot \left(\frac{\mathrm{d}^2 \vec{r}_0'}{\mathrm{d}t^2} - \vec{\Omega} \times \frac{\mathrm{d}\vec{r}_0'}{\mathrm{d}t} + \frac{\mathrm{d}\vec{\Omega}}{\mathrm{d}t} \times \vec{r} \right) - \nu \frac{\partial \omega'}{\partial \tau}, \tag{24}$$

in which we have dropped the index '1' for clarity.

The Neumann problem just derived is subject to a compatibility condition due to the behaviour at infinity requested by (23). If we denote the right-hand side of equation (24) by g, this condition can be written as

$$\int\int_D \mathrm{div}(\vec{\omega}' \times \vec{v}) \mathrm{d}x\mathrm{d}y + \int_{\partial D} g \, \mathrm{d}s = 0. \tag{25}$$

One can easily show that this is identically satisfied by applying the flux divergence theorem to the first term of equation (25). It is very important for the numerical procedure to maintain this property, otherwise the computed pressure will diverge at infinity as $\ln r$.

In a similar way we can derive a relation for the tangential derivative of H in the regular points of ∂D:

$$\frac{\partial H}{\partial \tau} = \frac{\partial \gamma}{\partial t} - \vec{r} \left(\frac{\mathrm{d}^2 \vec{r}_0'}{\mathrm{d}t^2} - \vec{\Omega} \times \frac{\mathrm{d}\vec{r}_0'}{\mathrm{d}t} + \frac{\mathrm{d}\vec{\Omega}}{\mathrm{d}t} \times \vec{r} \right) - \nu \frac{\partial \omega'}{\partial n}. \tag{26}$$

For physical reasons we shall impose that H be continuous over the profile trailing edge. By integration, after applying the Stokes theorem to the term containing $\mathrm{d}\vec{\Omega}/\mathrm{d}t$, this leads to

$$\frac{\mathrm{d}}{\mathrm{d}t} \int_{\partial D} \gamma \mathrm{d}s + 2 \frac{\mathrm{d}\Omega}{\mathrm{d}t} \mathrm{meas}\,(CD) - \nu \int_{\partial D} \frac{\partial \omega'}{\partial n} = 0. \tag{27}$$

On the other hand, integration of the vorticity transport and diffusion equation over D gives, after some simple transformations,

$$\frac{\mathrm{d}}{\mathrm{d}t} \int\int_D \omega' \mathrm{d}x\mathrm{d}y = \nu \int_{\partial D} \frac{\partial \omega'}{\partial n} \mathrm{d}s. \tag{28}$$

(This shows that when there is no advection flux through the domain boundary, the only way vorticity can enter is by diffusion from the solid surface.)

From (27) and (28), via integration in time, one obtains

$$\int\int_D \omega' \mathrm{d}x\mathrm{d}y + \int_{\partial D} \gamma \mathrm{d}s + 2\Omega \, \mathrm{meas}\,(CD) = \mathrm{const.}, \tag{29}$$

which represents the law of total vorticity conservation over D (if one takes (15) for the definition of vorticity over [2]). In particular, if the constant is zero at $t = 0$, it will remain so at any later time. We shall assume from now on that this is true for our case.

Now we are able to evaluate the constant C that appears in (18). It is well known from potential theory that for the Robin source distribution we have

$$\int_{\partial D} \gamma_R \mathrm{d}s \neq 0, \tag{30}$$

so we can always set C from

$$C = \left(\iint_D \omega' \mathrm{d}x\mathrm{d}y + \int_{\partial D} \gamma_0 \mathrm{d}s + 2\Omega \text{ meas } (CD) \right) \Big/ \int_{\partial D} \gamma_R \mathrm{d}s, \tag{31}$$

which completes the procedure for the bounded vorticity computation.

BOUNDARY CONDITION FOR VORTICITY

There are many local formulae for computing the boundary vorticity at solid surfaces from data inside the domain, most of them based on Taylor series expansions and interpolation techniques. Wu[5] gives a detailed discussion of such methods, showing that the first-order formulae do not account for the pressure gradient correctly while the second-order ones do not satisfy the vorticity conservation principle proved in the previous section. From his point of view this may be the cause of unstable behaviour of the latter.

Following these ideas, he proposes a way to compute the boundary vorticity using values of $\vec{\gamma}$ which ensure the impermeability of the solid wall. This bounded vorticity is considered to be uniformly spread over a distance equal to half the local spatial step in the direction normal to the solid wall, 'smearing out' the tangential velocity discontinuity. The values thus obtained are used as the boundary vorticity for the transport and diffusion equation. Bearing in mind the results of the previous section, it follows that the total vorticity conservation law is now satisfied. On the other hand, there is no local restriction on the normal derivative of the vorticity at the boundary, so the pressure gradient along the solid wall is free to develop.

However, when used with an implicit discretization for the transport and diffusion equation, this does not ensure the stability of the method, because the wall vorticity computed in this way fails to satisfy the implicit part of the discrete equation. It becomes necessary to employ underrelaxation techniques in an iterative algorithm performed at each time step in order to properly couple the transport and diffusion with the boundary vorticity computation formula. This is also done by El Refaee *et al.*[6] for the method extended to compressible flow.

An alternative method to underrelaxation is presented in References 8 and 9, in the framework of generalized formulations in Sobolev spaces, for the Stokes and Navier–Stokes problems. The authors construct a set of ω-fields that satisfy the impermeability condition at the wall, as well as the homogeneous equation formed with the implicit operator of the discretized transport and diffusion equation, and whose traces on the solid boundary form a basis of its discretized space. This basis is then used to correct the solution for the new time level in order to satisfy the no-slip condition while preserving the other two properties.

For an explicit finite difference method the implicit operator for interior points is the identity, so the method of Wu[5] is applicable without any other precautions. Taking into account its simplicity and improved behaviour over classical methods, as well as the advantage of confining the computational area to the viscous region of the flow, we decided on its use in the present research, together with the explicit difference scheme of Leonard (described in the section on the numerical procedure).

In the future we intend to develop a new method using characteristics for modelling the vorticity transport and an implicit finite difference scheme for the diffusion, with boundary conditions for vorticity imposed in a coupled manner as in References 8 and 9. The use of the Poincaré identity will preserve the advantage of confining the calculations to the viscous region of the flow. Alternatively, a finite element method can be devised on the same principle, employing the generalized form of the Poincaré identity described in References 10 and 11.

NUMERICAL PROCEDURE

Let us consider, as suggested in Reference 6, the conformal mapping $\zeta = \zeta(z)$ of the domain D onto the exterior of the unit circle (with $z = x + \mathrm{i}y$ in the profile plane and $\zeta = \xi + \mathrm{i}\eta$ in the circle plane). Denoting by v_ξ and v_η the covariant components of $\vec{v}$ in the curvilinear co-ordinate system defined by the conformal mapping, one obtains from equations (3a), (3c) and (12)

$$\frac{\partial v_\xi}{\partial \xi} + \frac{\partial v_\eta}{\partial \eta} = 0, \tag{32a}$$

$$\frac{\partial v_\eta}{\partial \xi} + \frac{\partial v_\xi}{\partial \eta} = \frac{\omega}{J} = \frac{\omega' - 2\Omega}{J}, \tag{32b}$$

$$\frac{\partial}{\partial t}\left(\frac{\omega'}{J}\right) + \frac{\partial}{\partial \xi}(v_\xi \omega') + \frac{\partial}{\partial \eta}(v_n \omega') = \nu\left(\frac{\partial^2 \omega'}{\partial \xi^2} + \frac{\partial^2 \omega'}{\partial \eta^2}\right), \tag{32c}$$

in which $J = \xi_x^2 + \xi_y^2$ is the Jacobian of the conformal mapping. Moreover, the boundary conditions are the same at infinity provided that $\mathrm{d}\zeta/\mathrm{d}z \to 1$ for $r \to \infty$. This suggests that we may consider a fictitious problem in the $\xi - \eta$ plane with v_ξ, v_η and ω' as unknown functions, very much like the original one but with advantageous geometric characteristics (for reasons we shall see later). In fact, it can be shown that one may obtain the covariant components of the velocity from equation (19) by replacing ω' by ω'/J, the x–y co-ordinates by ξ–η and the transport velocity terms by their covariant components in the new system according to

$$v_{\xi\infty} = \left(\frac{\mathrm{d}x_0'}{\mathrm{t}t}\cos\theta + \frac{\mathrm{d}y_0'}{\mathrm{d}t}\sin\theta\right)x_\xi + \left(-\frac{\mathrm{d}x_0'}{\mathrm{d}t}\sin\theta + \frac{\mathrm{d}y_0'}{\mathrm{d}t}\cos\theta\right)y_\xi - \Omega(xx_\eta + yy_\eta), \tag{33a}$$

$$v_{\eta\infty} = \left(\frac{\mathrm{d}x_0'}{\mathrm{d}t}\cos\theta + \frac{\mathrm{d}y_0'}{\mathrm{d}t}\sin\theta\right)x_\eta + \left(-\frac{\mathrm{d}x_0'}{\mathrm{d}t}\sin\theta + \frac{\mathrm{d}y_0'}{\mathrm{d}t}\cos\theta\right)y_\eta - \Omega(xx_\xi + yy_\xi). \tag{33b}$$

A similar procedure can be applied to the Fredholm integral equation (17). From now on we shall work in the circle plane and use the term 'velocity' for the vector defined in this plane by the covariant components v_ξ, and v_η.

Let ϱ and ϑ be a set of quasi-polar co-ordinates, allowing for mesh stretching in the radial direction, given by

$$\xi = \varphi = (\varrho)\cos\vartheta, \qquad \eta = \varphi(\varrho)\sin\vartheta, \tag{34}$$

in which φ: $[0, 1] \to [1, \infty]$ is a monotonically increasing function satisfying $\varphi(0) = 1$ and $\lim_{\vartheta\to}(\varrho) = \infty$ (in numerical practice the infinity will be replaced by a large enough radius $R_{\max}$). The vorticity transport and diffusion equation becomes

$$\frac{\partial}{\partial t}\left(\frac{\varphi\varphi'}{J}\Omega\right) + \frac{\partial}{\partial \varrho}(\varphi v_\varrho \omega) + \frac{\partial}{\partial \varrho}(\varphi' v_\varrho \omega) = \nu\left[\frac{\partial}{\partial \varrho}\left(\frac{\varphi}{\varphi'}\frac{\partial \omega}{\partial \varrho}\right) + \frac{\partial}{\partial \vartheta}\left(\frac{\varphi'}{\varphi}\frac{\partial \omega}{\partial \vartheta}\right)\right], \tag{35}$$

with v_ϱ and v_ϑ the (fictitious) velocity projections on the corresponding co-ordinate directions. For the velocity components we have

$$v_\varrho(\varrho,\vartheta) = -v_{\varrho\infty} + \frac{1}{2\pi}\int_0^{2\pi}\gamma(\vartheta_1)\frac{\sin(\vartheta_1-\vartheta)}{\varphi^2(\varrho)-2\varphi(\varrho)\cos(\vartheta-\vartheta_1)+1}\,\mathrm{d}\vartheta_1 + \frac{1}{2\pi}\int_0^1\int_0^{2\pi}\frac{\omega}{J}(\varrho_1,\vartheta_1)\frac{\varphi(\varrho_1)\sin(\vartheta_1-\vartheta)}{\varphi^2(\varrho)-2\varphi(\varrho)\varphi(\varrho_1)\cos(\vartheta-\vartheta_1)+\varphi^2(\varrho_1)}\varphi(\varrho_1)\varphi'(\varrho_1)\mathrm{d}\varrho_1\mathrm{d}\vartheta_1, \quad (36a)$$

$$v_\varrho(\varrho,\vartheta) = -v_\varrho\infty + \frac{1}{2\pi}\int_0^{2\pi}\gamma(\vartheta_1)\frac{\varphi)-\cos(\vartheta_1-\vartheta)}{\varphi^2(\varrho)-2\varphi(\varrho)\cos(\vartheta-\vartheta_1)+1}\,\mathrm{d}\vartheta_1 + \frac{1}{2\pi}\int_0^1\int_0^{2\pi}\frac{\omega}{J}(\varrho_1,\vartheta_1)\frac{\varphi(\varrho)-\varphi(\varrho_1)\cos(\vartheta_1-\vartheta)}{\varphi^2(\varrho)-2\varphi(\varrho)\varphi(\varrho_1)\cos(\vartheta-\vartheta_1)+\varphi^2(\varrho_1)}\varphi(\varrho_1)\varphi'(\varrho_1)\mathrm{d}\varrho_1\mathrm{d}\vartheta_1, \quad (36b)$$

in which $v_{\varrho\infty}$ and $v_{\vartheta\infty}$ are the projections in the directions ς and ϑ respectively of the velocity vector $(v_{\xi\infty},\ v_{\eta\infty})$ defined above.

Suppose that we have divided the computational domain into equal intervals in the ϑ-direction. We shall take, as suggested in Reference 6, the following expressions for the free and the bounded vorticity respectively:

$$\frac{\varphi\varphi'\omega}{J}(\varrho,\vartheta) = \tfrac{1}{2}A_0(\varrho) + \sum_{k=1}^{N}[A_k(\varrho)\cos(k\varrho) + B_k(\varrho)\sin(k\vartheta)], \quad (37a)$$

$$\gamma(\vartheta) = \tfrac{1}{2}a_0 + \sum_{k=1}^{N}[a_k\cos(k\vartheta) + b_k\sin(k\vartheta)]. \quad (37b)$$

The integrals in the ϑ-direction can now be evaluated using the residuum theorem. One obtains

$$v_\varrho(\varrho,\vartheta) = -v_{\varrho\infty} + \frac{1}{2\varphi(\varrho)}\sum_{k=0}^{N}\left(\frac{b_k}{\varphi^k(\varrho)}\cos(k\vartheta) - \frac{a_k}{\varphi^k(\varrho)}\sin(k\vartheta)\right) + \frac{1}{2\varphi(\varrho)}\sum_{k=1}^{N}\{[I_B^K(\varrho)+J_B^k(\varrho)]\cos(k\vartheta) - [I_A^k(\varrho)+J_A^k(\varrho)]\sin(k\vartheta)\}, \quad (38a)$$

$$v_\varrho(\varrho,\vartheta) = -v_{\varrho\infty} + \frac{1}{2\varphi(\varrho)}\sum_{k=0}^{N}\left(\frac{a_k}{\varphi^k(\varrho)}\cos(k\vartheta) - \frac{b_k}{\varphi^k(\varrho)}\sin(k\vartheta)\right) + \frac{1}{2\varphi(\varrho)}\left(I_A^0 + \sum_{k=1}^{N}\{[I_A^K(\varrho)-J_A^k(\varrho)]\cos(k\vartheta) + [I_B^k(\varrho)-J_B^k(\varrho)]\sin(k\vartheta)\}\right), \quad (38b)$$

with

$$I_A^k(\varrho) = \int_0^{\varrho}\left(\frac{\varphi(\varrho_1)}{\varphi(\varrho)}\right)^k A_k(\varrho_1)\mathrm{d}\varrho_1, \quad k=0,\ldots,N, \quad (39a)$$

$$J_A^k(\varrho) = \int_{\varrho}^{1}\left(\frac{\varphi(\varrho)}{\varphi(\varrho_1)}\right)^k A_k(\varrho_1)\mathrm{d}\varrho_1, \quad k=0,\ldots,N, \quad (39b)$$

and similar expressions for I_B^k and J_B^k. At this point we can see an advantage resulting from the use of the conformal mapping: it allows us to change the form (19) of the velocity representation to (38), in which the singularities are eliminated by integration in the ϑ-direction. The integrals in the ϱ-direction can now be easily evaluated by the usual numerical procedures, e.g. by the trapezoidal rule.

However, the main advantage lies in the properties related to the Fredholm integral equation (17). In the first place the Robin potential for the circle is induced by a constant source distribution. With γ_R constant, imposition of the total vorticity conservation law is achieved by simply distributing the

vorticity excess from equation (31) uniformly over the circumference. Moreover, when we look for a solution γ_0 of zero mean value (which is equivalent to considering $a_0 = 0$ in (38a)), the integral in the left-hand member of equation (17) vanishes and the Fredholm integral equation becomes an explicit formula for boundary vorticity computation:

$$\gamma_0(\vartheta) = -2v_{\vartheta\infty} - \sum_{k=1}^{N} [J_A^k(0)\cos(k\vartheta) + J_B^k(0)\sin(k\vartheta)]. \tag{40}$$

This outstanding property of the circle considerably simplifies the numerical algorithm and is the main reason for the conformal mapping usage.

The vorticity transport and diffusion equation (35) is discretized using an explicit scheme with high-order upwind differencing for the advection terms and the usual centred differencing for the diffusion ones (see Reference 12, the algorithm of Leonard (1979)). The scheme can be written in flux terms as

$$\frac{1}{\Delta t}\left[\left(\frac{\omega\varphi\varphi'}{J}\right)_{i,j}^{n+1} - \left(\frac{\omega\varphi\varphi'}{J}\right)_{i,j}^{n}\right] = \frac{1}{\Delta\vartheta}[(FH)_{i+1/2,j}^{n} - (FH)_{i-1/2,j}^{n}] + \frac{1}{\Delta\varrho}[(FV)_{i,j+1/2}^{n} - (FV)_{i,j-1/2}^{n}] \tag{41}$$

and the fluxes are given by

$$(FH)_{i+1/2,j} = \begin{cases} -\left(\dfrac{J}{\varphi}v_\vartheta\right)_{i+1/2,j}\left(\dfrac{\tilde\omega_{i+1,j}+\tilde\omega_{i,j}}{2} - \dfrac{q}{3}(\tilde\omega_{i+1,j} - 2\tilde\omega_{i,j} + \tilde\omega_{i-1,j})\right) \\ +\nu\left(\dfrac{\varphi'}{\varphi}\right)_{i+1/2,j}\dfrac{\omega_{i+1,j}-\omega_{i,j}}{\Delta\vartheta} \quad \text{for} \quad (v_\vartheta)_{i+1/2,j} > 0, \\ -\left(\dfrac{J}{\varphi}v_\vartheta\right)_{i+1/2,j}\left(\dfrac{\tilde\omega_{i+1,j}+\tilde\omega_{i,j}}{2} - \dfrac{q}{3}(\tilde\omega_{i+2,j} - 2\tilde\omega_{i+1,j} + \tilde\omega_{i,j})\right) \\ +\nu\left(\dfrac{\varphi'}{\varphi}\right)_{i+1/2,j}\dfrac{\omega_{i+1,j}-\omega_{i,j}}{\Delta\vartheta} \quad \text{for} \quad (v_\vartheta)_{i+1/2,j} < 0, \end{cases} \tag{42}$$

$$(FV)_{i,j+1/2} = \begin{cases} -\left(\dfrac{J}{\varphi'}v_\vartheta\right)_{i,j+1/2}\left(\dfrac{\tilde\omega_{i,j+1}+\tilde\omega_{i,j}}{2} - \dfrac{q}{3}(\tilde\omega_{i,j+1} - 2\tilde\omega_{i,j} + \tilde\omega_{i,j-1})\right) \\ +\nu\left(\dfrac{\varphi}{\varphi'}\right)_{i,j+1/2}\dfrac{\omega_{i,j+1}-\omega_{i,j}}{\Delta\vartheta} \quad \text{for} \quad (v_\vartheta)_{i,j+1/2} > 0, \\ -\left(\dfrac{J}{\varphi'}v_\varrho\right)_{i,j+1/2}\left(\dfrac{\tilde\omega_{i,j+1}+\tilde\omega_{i,j}}{2} - \dfrac{q}{3}(\tilde\omega_{i,j+2} - 2\tilde\omega_{i,j+1} + \tilde\omega_{i,j})\right) \\ +\nu\left(\dfrac{\varphi}{\varphi'}\right)_{i,j+1/2}\dfrac{\omega_{i,j+1}-\omega_{i,j}}{\Delta\varrho} \quad \text{for} \quad (v_\vartheta)_{i,j+1/2} < 0, \end{cases} \tag{43}$$

with $\tilde\omega = \varphi\varphi'\omega'/J$. Here q is chosen to increase accuracy (0·5) or to optimize steady state flow computation (0·375, the QUICK scheme of Leonard). This discretization, which makes use of the transport velocities related to the computational co-ordinate system, was found to have much better behaviour than the more straightforward one derived directly from (35) with $\varphi' v_\vartheta$ and φv_ϱ as transport velocities.

The stability criterion is the same as for the first-order upwind scheme; for two-dimensional flows we have used

$$\Delta t < \frac{1}{Jv_\varrho/\varphi'\Delta\varrho + Jv_\vartheta/\varphi\Delta\vartheta + 2Jv/(\varphi'\Delta\varrho)^2 + 2Jv/(\varphi\Delta\vartheta)^2}. \tag{44}$$

The vorticity on the solid boundary is computed using values of γ as indicated in the previous section. The formula is

$$\omega_{i,1} = \frac{2}{\varphi'\Delta\varrho}\gamma_i. \tag{45}$$

A special technique is employed in order to reduce storage requirements. Only the non-zero vorticity field is stored in a one-dimensional compact array, provided with a data structure that allows the programme to restore the original distribution only in the work area, for the finite difference scheme application. Only new vorticity values greater in modulus than a 'threshold' value established by the user are stored in the compact array for the vorticity at the new time level. The velocities are computed, when needed, from equations (38), so the whole velocity field storage is no longer necessary. However, one must keep in memory the values of coefficients A_k and B_k for the whole mesh, which, besides geometry data, involves most of the memory requirements of the programme.

Equations for pressure analogues to (22), (24) and (26) can be derived for the fictitious problem in the circle plane. The Bernoulli variable becomes

$$H = \frac{p}{\rho} + \frac{J}{2}(v_\xi^2 + v_\eta^2) - \frac{p_\infty}{\rho} - \frac{J}{2}(v_{\xi\infty}^2 + v_{\eta\infty}^2). \tag{46}$$

One obtains, after passing to ξ–η variables,

$$\Delta H = \frac{1}{\varphi\varphi'}\left(\frac{\partial}{\partial\varrho}(\varphi v_\vartheta\omega') - \frac{\partial}{\partial\vartheta}(\varphi' v_\varrho\omega')\right) \tag{47}$$

and for the first-order derivatives

$$\frac{1}{\varphi'}\frac{\partial H}{\partial\varrho} = -a_{\varrho\infty} - \frac{\partial v_\varrho}{\partial t} - v_\vartheta\omega' + \nu\frac{1}{\varphi}\frac{\partial\omega'}{\partial\vartheta}, \tag{48a}$$

$$\frac{1}{\varphi'}\frac{\partial H}{\partial\varrho} = -a_{\vartheta\infty} - \frac{\partial v_\vartheta}{\partial t} + v_\varrho\omega' - \nu\frac{1}{\varphi'}\frac{\partial\omega'}{\partial\varrho}, \tag{48b}$$

where $\vec{a}_{\varrho\infty}$ and $\vec{a}_{\vartheta\infty}$ correspond to the covariant components of the acceleration-type terms $\mathrm{d}^2\vec{r}_0'/\mathrm{d}t^2 - \Omega \times \mathrm{d}\vec{r}_0'/\mathrm{d}t + \mathrm{d}\vec{\Omega}/\mathrm{d}t \times \vec{r}$ given by the movement of the mobile system and projected on its axes (similar to transport velocities).

In the early stages of programme development the right-hand side members of equations (47) and (48) were evaluated from the known solution at the corresponding time level by centred finite differences in the directions ϱ and ϑ. A better (and more efficient) approach consists of using the fluxes defined previously (equations (45) and (46)) according to the relations

$$\left(\frac{1}{\varphi'}\frac{\partial H}{\partial\varrho}\right)_{i+1/2,j} = \left(-a_{\varrho\infty} - \frac{\partial v_\varrho}{\partial t} + \frac{1}{\varphi'}FH\right)_{i+1/2,j}, \tag{49a}$$

$$\left(\frac{1}{\varphi}\frac{\partial H}{\partial\vartheta}\right)_{i,j+1/2} = \left(-a_{\vartheta\infty} - \frac{\partial v_\vartheta}{\partial t} - \frac{1}{\varphi}FV\right)_{i,j+1/2} \tag{49b}$$

allowing us to write

$$(\Delta H)_{i+1/2,j+1/2} = \frac{1}{\varphi\varphi'}\left\{\frac{1}{\Delta\varrho}\left[\left(\frac{\varphi}{\varphi'(FH)}\right)_{i+1/2,j+1} - \left(\frac{\varphi}{\varphi'(FH)}\right)_{i+1/2,j}\right]\right.$$
$$\left. = \frac{1}{\Delta\vartheta}\left[\left(\frac{\varphi'}{\varphi(FV)}\right)_{i+1,j+1/2} - \left(\frac{\varphi'}{\varphi(FV)}\right)_{i,j+1/2}\right]\right\} \tag{50}$$

for all $i = 1, \ldots, n_\vartheta$ and $j = 1, \ldots, n_\varrho$, the discretized divergence of acceleration terms being neglected by virtue of their theoretical properties.

A Neumann problem can be written for H by considering (47) or (50) and applying (48a) or (49a) for $\varrho = 0$ or $j = 1$ respectively. In the second case, noting that the right-hand terms involve the horizontal fluxes at $j = 1$ and that the solution does not effectively depend on them (this is typical for Neumann problems constructed with gradients of the unknown function: the influence of the normal derivative at the boundary is cancelled by the surface-distributed source in its immediate proximity), we may simply set them to zero in both the boundary normal derivative and equation (50) written for $j = 1$.

As stated earlier care must be taken in satisfying the compatibility condition in both variants to avoid solution divergence at infinity. This implies in the first place that one should use an integration method compatible with the discretized derivative used in (47) or (50). Moreover, since the computational domain is bounded and therefore the vorticity will not be null at the outflow boundary, a fictitious row of surface-distributed sources must be considered to take into account the neglected part of the wake. This is achieved by applying (47) or (50) with a supplementary row of zero vorticity outside the mesh. For low Reynolds numbers such as 40, ignoring this problem will result in pressure shifts of as much as 50 per cent of the correct values.

A technique similar to that used for velocity computation is employed (Fourier series for the ϑ-direction and numerical integration (trapezoidal rule) for the ϱ-direction). The corresponding Fourier series for the source terms are

$$\varphi\varphi'\Delta H = \tfrac{1}{2}A_0(\varrho) + \sum_{k=1}^{N}[A_k(\varrho)\cos(k\vartheta) + B_k(\varrho)\sin(k\vartheta)], \tag{51}$$

$$\left(\frac{\varphi}{\varphi'}\frac{\partial H}{\partial\varrho}\right)_{\varrho=0} = \tfrac{1}{2}a_0 + \sum_{k=1}^{N}[a_k\cos(k\vartheta) + b_k\sin(k\vartheta)]. \tag{52}$$

The property of the circle highlighted above (for velocity computation) allows us to write the solution in terms of surface and single-layer potentials without solving any Fredholm integral equation. One obtains, after integrating with the residuum theorem in the ϑ-direction,

$$\frac{p(\varrho,\vartheta)}{\rho} = \frac{p_\infty}{\rho} + \frac{J}{2}(v_{\varrho\infty}^2 + v_{\vartheta\infty}^2) - \frac{J}{2}(v_\varrho^2 + v_\vartheta^2) + \tfrac{1}{2}a_0E_0(0,\varrho) + \tfrac{1}{2}\int_0^1 A_0(\varrho_1)E_0(\varrho_1,\varrho)\mathrm{d}\varrho_1$$
$$- \sum_{k=1}^{N}\frac{1}{2k}\left(\alpha_kE_k(0,\varrho) + \int_0^1 A_k(\varrho_1)E_k(\varrho_1,\varrho)\mathrm{d}\varrho_1\right)\cos(k\vartheta)$$
$$- \sum_{k=1}^{N}\frac{1}{2k}\left(\beta_kE_k(0,\varrho) + \int_0^1 B_k(\varrho_1)E_k(\varrho_1,\varrho)\mathrm{d}\varrho_1\right)\sin(k\vartheta), \tag{53}$$

in which α_k and β_k are given by

$$\alpha_k = 2a_k + \int_0^1 A_k(\varrho)1)E_k(\varrho_1,0)\mathrm{d}\varrho_1, \qquad \beta_k = 2b_k + \int_0^1 B_k(\varrho)E_k(\varrho_1,0)\mathrm{d}\varrho_1 \tag{54}$$

and E_k stand for

$$E_0(\varrho_1, \varrho) = \left\{ \begin{array}{ll} \ln \varphi(\varrho) & \text{for} \quad \varrho \geq \varrho_1 \\ \ln \varphi(\varrho_1) & \text{for} \quad \varrho < \varrho_1 \end{array} \right\} \quad \text{for} \quad k = 0, \tag{55a}$$

$$E_k(\varrho_1, \varrho) = \left\{ \begin{array}{ll} [\varphi(\varrho_1)/\varphi(\varrho)]^k & \text{for} \quad \varrho \geq \varrho_1 \\ [\varphi(\varrho)/\varphi(\varrho_1)]^k & \text{for} \quad \varrho < \varrho_1 \end{array} \right\} \quad \text{for} \quad k = 1, \ldots, N. \tag{55b}$$

An alternative method of pressure computation consists of integrating, relative to ϑ, equation (48b) (or (49b)) written for points on the boundary. If one wants to maintain the uniformity of H in the numerical scheme by virtue of discretized total vorticity law conservation, equation (49b) must be used written as

$$\left(\frac{\partial H}{\partial \vartheta}\right)^n_{i,1} = -(a_{\vartheta\infty})^n_{i,1} - \frac{\gamma_i^{n+1}}{\Delta t} - (FV)_{i,3/2}. \tag{56}$$

As one can see, the tangential velocity time derivative is computed by the difference between the tangential velocity induced by the new vorticity field in the presence of the impermeable (in the mobile frame) body and before imposing the no-slip condition, and the tangential velocity given by the old vorticity field, zero since the latter has already been subjected to this condition. Summing equation (56) over all the boundary yields the numerical equivalent of the total vorticity conservation law (29) provided that the evaluation of its right-hand side is made using the same fluxes FV as the (conservative) finite difference scheme (41)–(43) for points on the second row.

The integration is performed in the spectral domain; the above considerations show that the constant component of the right-hand side identically vanishes. As will be shown in the next section, the values given by this method are closer to the results of the Neumann problem than the ones obtained in a more straightforward way which cancels the $\partial v_\vartheta/\partial t$ (by virtue of the no-slip boundary condition), especially when high accelerations are imparted to the profile.

RESULTS

The first test case chosen was the steady flow around a circular cylinder at Reynolds number 40. A 128×60 polar mesh was used, extended to a maximum radius of 12·5 (all dimensions are related to the cylinder diameter) stretched towards the cylinder surface. The comparison results were taken from experimental data of Grove *et al.*[13] Figure 2 shows the streamline pattern. The drawn level values are stretched towards the reference value on the solid surface, allowing a better visualization of the wake details. One can measure the wake parameters and a comparison with the experimental ones shows a good coincidence. For example, the computed wake length (measured from the cylinder to the junction of downstream lines) gives an approximate value of 2·55 compared with 2·75. The position of the wake vertex centre relative to the cylinder axis is (from a raw measurement) (1·2, 0·3) compared with (1·2, 0·32). The pressure values are shown in Figure 3. Both methods for discretizing the source terms of the pressure Neumann problem give almost the same results (the 'global computed pressure' curve), showing a good coincidence with the measured ones. The results of the local method are also in good agreement with the global one and even better with experiment, provided that an appropriate translation is made. The computed pressure, friction and total drag coefficients are respectively 1·04, 0·53 and 1·57; the last is to be compared with the experimental value of 1·60.

For the non-stationary movement we have chosen the case of a 20 per cent thick elliptic profile performing an oscillatory translation and rotation movement in viscous fluid, superposed over a

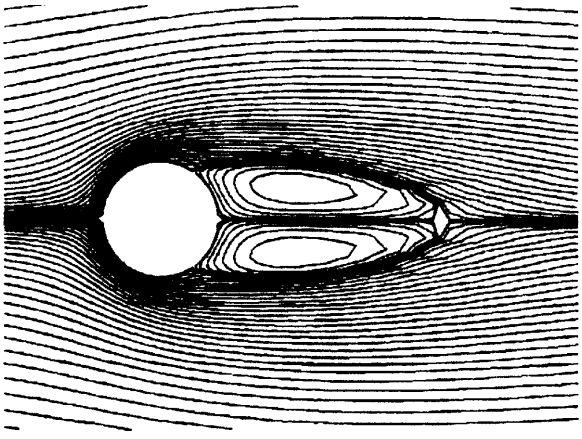

Figure 2

uniform one along the Ox' axis in its negative sense. In the following considerations all parameters are adimensionalized with respect to the ellipse chord size and the velocity of the uniform movement and the classical definitions were taken for force and moment coefficients.

The Reynolds number is 40. We have chosen two types of movement: an oscillatory translation with a vertical velocity amplitude of 0·1 (called from now on 'translation') and a combination of translation and rotation, in which a rotation oscillation is added, with the same frequency, an angular amplitude of 0·05 rad (2·9°) and an opposite phase (called from now on 'rotation'). For each, three (adimensional) frequencies were considered: 0·0795, 0·1592 and 0·3183. The same cases were chosen in Reference 14 and a comparison with the results therein will be made. We shall also call, for convenience, a 'separation point' any point on the profile surface for which $\omega = 0$, although this is somewhat inappropriate for the leading edge impact point.

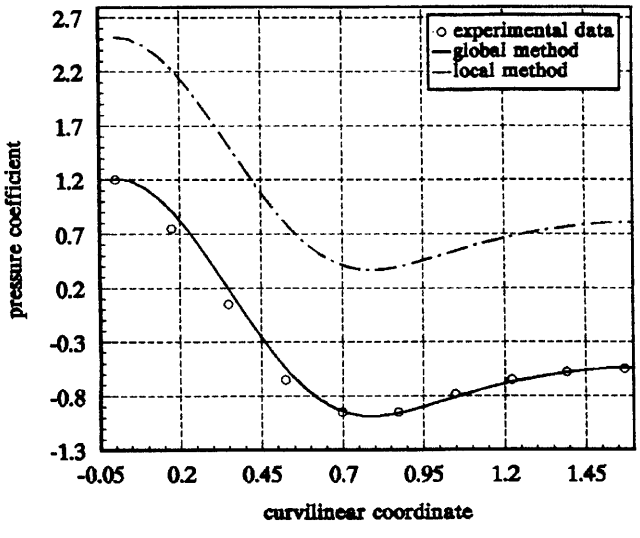

Figure 3

The non-stationary movement starts with the profile in uniform movement at zero incidence, for which the flow has been previously computed.

Theoretical calculations were performed for the inviscid case under the hypothesis of zero circulation movement. In fact, if one prevents the vorticity appearance by blocking the no-slip boundary condition application, the programme simulates such a flow by virtue of the total vorticity conservation law, involving in this case only the profile inner vorticity and the bounded one.

Figures 4 and 7 show a synoptic image of the lift coefficient variation (the most representative) for the highest-frequency case. As expected, the inviscid case yields zero average lift; the period vertical force is a virtual mass effect. On the other hand, the stationary viscous flow exhibits a lift force, showing that a non-zero circulation is created around the profile. However, it is only half the value predicted by applying the Kutta condition at the trailing edge and this is caused by its rounded form as well as by the low Reynolds number.

For the translation case, 'summing' the mentioned curves yields approximately the curve for oscillatory movement in viscous fluid. This means that the non-stationary influence is essentially limited to virtual mass effects; for the rest the flow establishes the lift corresponding to the current incidence value in a quasi-stationary manner. A comparison between different methods of pressure computation shows a good coincidence. As stated in the previous section, the use of the $\partial\gamma/\partial t$ (local method 2) term slightly improves the results over the usual approach (local method 1). These results are in good agreement with Reference 14, except for a factor of two; this is due, in our opinion, to an adimensionalization inadvertence (the lift coefficient is probably adimensionalized with respect to ρv^2 instead of $\rho v^2/2$).

The separation point evolution diagrams for the translation case are shown in Figures 5 and 6. While the leading edge point position does not differ much from inviscid flow theoretical predictions, the trailing edge point is more influenced by the viscous effects and thus larger differences occur, as one would expect. The separation point diagrams are in good agreement with Reference 14.

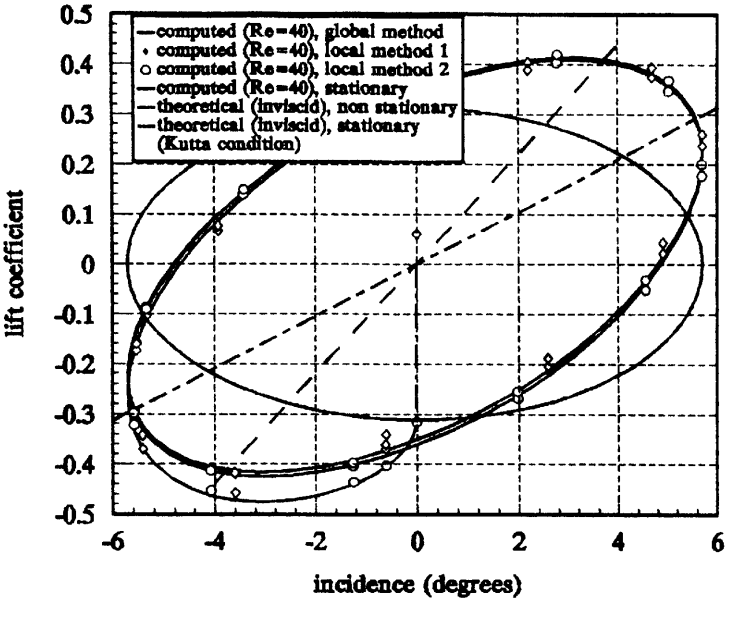

Figure 4

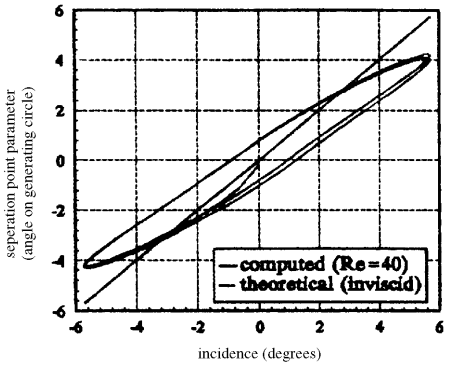

Figure 5

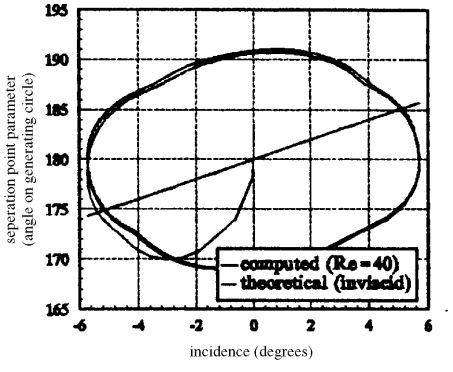

Figure 6

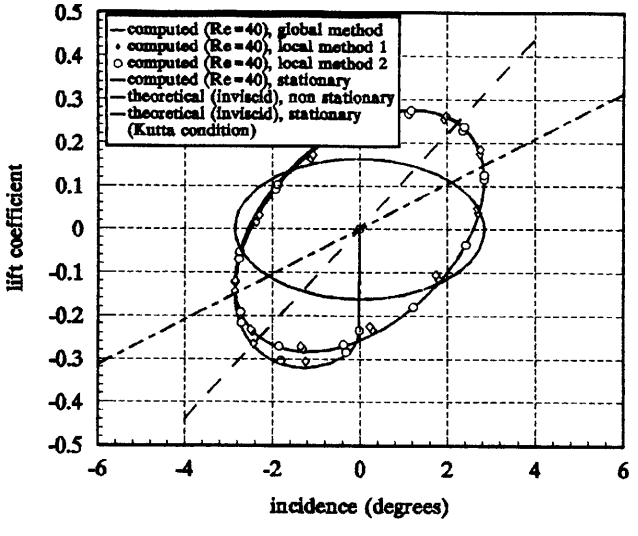

Figure 7

Similar considerations apply to the rotation case. However, some differences appear owing to the influence of rotation on the circulation behaviour; for example the 'sum' of theoretical non-stationary lift and stationary lift for viscous flow does not yield any longer the lift curve for non-stationary real movement.

A discontinuity in the separation point position appears owing to a discontinuity in the angular velocity value Ω at the start of the oscillatory movement, which in turn gives a discontinuity in the bounded circulation value (constant C in equation (18)). It is rapidly damped for the leading edge point but persists for a longer time for the trailing edge one (see Figures 8 and 9), where the vorticity transport is slower.

No such phenomena are shown in Reference 14 and the coincidence is less accurate. Our results indicate a more regular shape of the leading edge separation point curve with a smaller amplitude (approximately 3° in comparison with 5°). These differences probably result from the different ways of choosing the bounded circulation value (which, for Reference 14, means choosing an appropriate streamfunction solution for a given vorticity field). Oshima *et al.*[14] do not make any reference to the total vorticity conservation law; they compute the streamfunction as the sum of a potential term, corresponding to the zero-circulation inviscid movement around the ellipse, and a perturbation term, given by the vorticity field and also yielding zero circulation on the profile surface. This is equivalent to setting $C = 0$ in (18) and may be the cause of the difference in the results.

However, we think that the discontinuity is overestimated owing to the explicit character of this method. Indeed, a change in movement parameters at time level n is reflected in the boundary conditions, while the interior vorticity values are computed using the old velocities (with old movement parameters). Such delays introduce only $O(\Delta t)$ errors in the numerical scheme, which is unimportant when Δt is very small (and this is our case, because of the CFL stability requirement) and the variable variation is sufficiently regular, but may become important when we deal with discontinuities.

Figures 10 and 11 show the lift hysteresis curves for all three frequencies. It can be seen that there is an almost proportional relationship between the hysteresis phenomenon amplitude and the frequency and this may be correlated with the fact that no separation phenomena occur, so that the profile acceleration effects remain predominant. Again, while the translation case shows a good coincidence with Reference 14 (regardless of the factor of two mentioned earlier), the rotation case

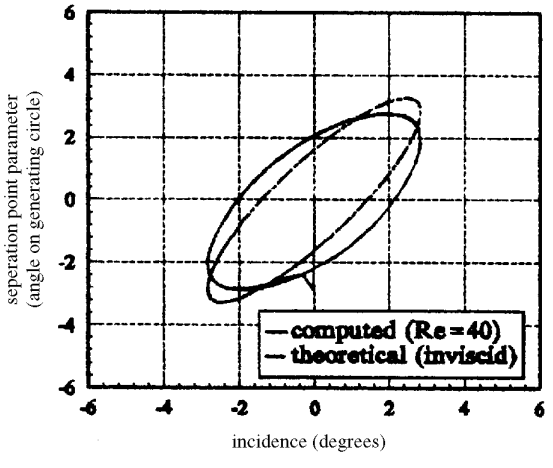

Figure 8

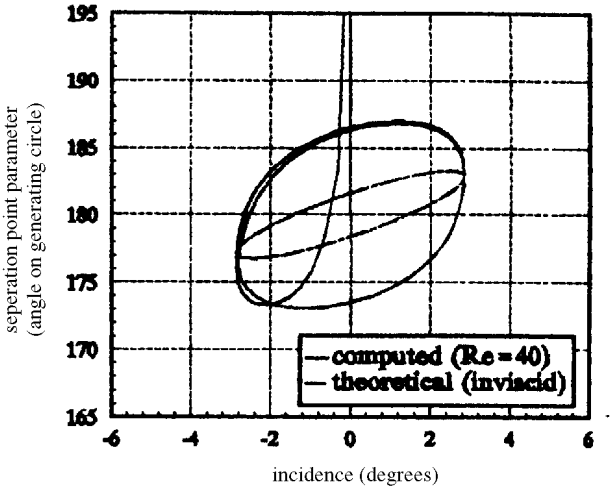

Figure 9

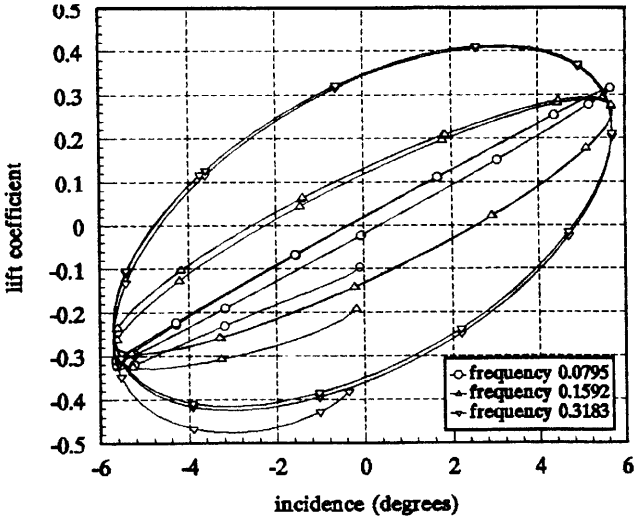

Figure 10

does not yield the same accuracy; in particular, the proportionality mentioned above does not hold for results presented therein. In other respects (e.g. lift amplitude) the agreement is rather good, with no need for the adimensionalization correction coefficient of two.

In this form the method did not allow for high-Reynolds-number flow treatment. For this purpose it must be improved by introducing an implicit scheme in order to transcend the CFL stability condition, which is very restrictive when fine meshes are used.

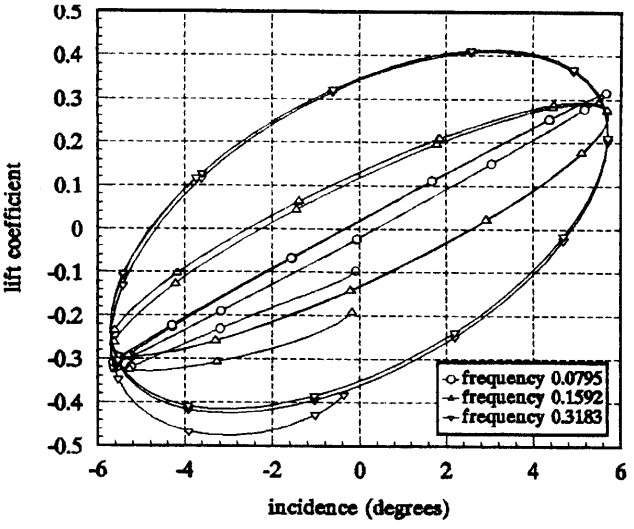

Figure 11

CONCLUSIONS

This is a first step towards the proposed aim of computing the viscous flow around a moving profile. The examples presented in the previous section validate the method and programme for laminar flows, at least for low Reynolds numbers.

Although in this form the programme allows for memory and computing time savings by reducing the computational domain, we feel that a finite element formulation is more suitable for this purpose.

A turbulence model must be used to compute the high-Reynolds-number flows useful for applications. Following Reference 6, compressibility corrections could not be added, thus completing the procedure for helicopter blade non-stationary flow simulation (under the assumption of blade element plane flow).

REFERENCES

1. J. M. Currier, K. Y. Young and K. Y. Fung, 'Analysis of the onset of dynamical stall', *AIAA J.*, **30**, (1992).
2. M. Acharya and M. H. Metwally, 'Unsteady pressure field and vorticity production over a pitching airfoil'. *AIAA J.*, **30**, (1992).
3. C. Shih, L. Lourenco, L. Van Dommelen and A. Krothapalli, 'Unsteady flow past an airfoil pitching at a constant rate', *AIAA J.*, **30**, (1992).
4. T. Reu and S. X. Ying, 'Hybrid grid approach to study dynamic stall', *AIAA J.*, **30**, (1992).
5. J. C. Wu, 'Numerical boundary conditions for viscous flow problems', *AIAA J.*, **14**, (1976).
6. M. M. El Refaee, J. C. Wu and S. G. Lekoudis, 'Solution of the compressible Navier–Stokes equations using the integral method', *AIAA J.*, **20**, (1982).
7. P. J. Roache, *Computational Fluid Dynamics*, Hermosa, Albuquerque, NM, 1976.
8. O. Pironneau and R. Glowinski, 'Numerical methods for the first biharmonic equation and for the two-dimensional Stokes problem', *SIAM Rev.*, **21**, (1979).
9. O. Pironneau, R. Glowinski and Y. Achdou, 'Tuning the mesh of a mixed method for the Navier–Stokes equations', *Rapports de Recherche INRIA 1514*, 1991.
10. P. Bassanini, C. M. Casciola, M. R. Lancia and R. Piva, 'A boundary integral formulation for the kinetic field in aerodynamics, Part I, Mathematical analysis', *Eur. J. Mech. B.*, **10**, (1991).
11. P. Bassanini, C. M. Casciola, M. R. Lancia and R. Piva, 'A boundary integral formulation for the kinetic field in aerodynamics, Part II, Applications to unsteady 2D flow', *Eur. J. Mech. B.*, **11**, (1992).

12. C. A. J. Fletcher, *Computational Techniques for Fluid Dynamics*, Springer, New York, 1998.
13. A. S. Grove, F. H. Shair, E. E., Petersen and A. Acrivos, 'An experimental investigation of steady separated flow past a circular cylinder', *J. Fluid Mech*., **33**, (1964).
14. K. Oshima, Y. Oshima and Y. Kuriyama, 'Finite element analysis of viscous incompressible flow around an oscillating airfoil',

